



One-dimensional CdS@MoS₂ core-shell nanowires for boosted photocatalytic hydrogen evolution under visible light

Bin Han^a, Siqi Liu^{a,b}, Nan Zhang^{a,b}, Yi-Jun Xu^{a,b,*}, Zi-Rong Tang^{a,*}

^a College of Chemistry, New Campus, Fuzhou University, Fuzhou, 350116, PR China

^b State Key Laboratory of Photocatalysis on Energy and Environment, College of Chemistry, Fuzhou University, Fuzhou, 350002, PR China

ARTICLE INFO

Article history:

Received 1 June 2016

Received in revised form 2 September 2016

Accepted 12 September 2016

Available online 14 September 2016

Keywords:

Core-shell

Nanowires

CdS

MoS₂

Photocatalytic hydrogen evolution

ABSTRACT

The well-defined one-dimensional (1D) CdS@MoS₂ (CM) core-shell nanowires are constructed by employing CdS nanowires (CdS NWs) as nanobuilding blocks via a facile hydrothermal strategy. The synergistic interaction, stemming from the large and intimate coaxial interfacial contact between MoS₂ thin shell and 1D CdS core, can efficiently retard the charge carrier recombination and the MoS₂ as noble-metal-free cocatalyst enriches the active sites for H₂ evolution from water. Consequently, in comparison to bare CdS nanowires, the resultant 1D core-shell CM composite exhibits distinctly enhanced visible light activity for the evolution of H₂. Notably, the activity of 1D CM with the optimized 2 wt% of MoS₂ exceeds that of pure CdS and CdS-1 wt% Pt composite by a factor of 64 and 4 times, respectively, under identical reaction conditions, while the apparent quantum yield (A.Q.Y.) at 420 nm over 1D CM reaches 28.5%. This work provides a simple paradigm for facile and finely controlled synthesis of well-shaped 1D-based composite photocatalysts towards boosted solar energy conversion.

© 2016 Elsevier B.V. All rights reserved.

1. Introduction

Splitting water into H₂ using semiconductor photocatalysts and solar energy has been regarded as a viable and sustainable solution with potential to address the increasing environmental and energy issues [1]. Since the first discovery of photo-electrochemical water splitting on a TiO₂ electrode [2], various photocatalysts have been extensively developed for H₂ production [3–10]. Among them, one-dimension (1D)-based semiconducting nanostructures, e.g., nanowires (NWs), nanorods (NRs) and nanotubes (NTs), have stirred mounting interests due to their intrinsic structural and electronic characteristics of large surface area with high length-to-diameter ratios, considerably higher electron mobility and vectorial electron transport with short radial distances [11–18]. For instance, very recently, Yu et al. have demonstrated that CdS NWs exhibit a higher photocatalytic H₂ evolution rate than its counterparts with other morphologies [19]. However, despite the fact that diverse 1D semiconductor photocatalysts have been constructed, almost no single one is able to impart efficient H₂ evolution activity even in the presence of sacrificial agent [20–23], which is still a critical ob-

stacle to the wide practical application of 1D-based semiconductor photocatalysts.

To improve the photocatalytic activity for H₂ evolution, loading appropriate cocatalysts onto the surface of the photocatalysts has proven to be an effectual strategy [24–29]. In the hydrogen evolution reaction (HER), appropriate cocatalysts can significantly facilitate the reactions by synergistic effects of enriching the active sites, suppressing the charge recombination and reverse reactions, as well as lowering the activation energy [30–33]. Recent studies have demonstrated that MoS₂, a transition metal sulfide consisting of three atom layers (S-Mo-S) stacking together via weak van der Waals interaction, is in a position to perform as an efficient cocatalyst for H₂ production due to the existence of abundant active sites stemming from the sulfur edge [34–40]. Additionally, the merits of earth-abundance, low cost, and nontoxicity outline the great potential for its widespread application in future hydrogen economy [41–47]. It is, therefore, of considerable interest to develop 1D semiconductors-MoS₂ hybrid photocatalysts with high activity and good durability for photocatalytic H₂ production.

Herein, 1D CdS NWs are employed as nanoscale building blocks for the construction of 1D CdS NWs@MoS₂ (CM) hybrid photocatalyst due to its desirable band gap ($E_g \approx 2.40$ eV) for absorption of visible light and suitable conduction band edge positions for H₂ evolution. The resultant well-shaped 1D core-shell structure provides large and intimate coaxial interfacial contact between MoS₂

* Corresponding authors.

E-mail addresses: yjxu@fzu.edu.cn (Y.-J. Xu), zrtang@fzu.edu.cn (Z.-R. Tang).

thin shell and 1D CdS core, thus promoting the transfer of photo-generated electrons from semiconductor core to MoS_2 thin shell. The 1D CM composite exhibits distinctly enhanced photocatalytic activity in comparison with both CdS NWs and CdS-Pt composites, and the heterostructure with optimal loading amount exhibits a H_2 evolution rate of $493.1 \mu\text{mol h}^{-1}$ with an apparent quantum yield (A.Q.Y.) of 28.5% at 420 nm. It is anticipated that this work could potentially provide a new stepping stone for designing well-shaped 1D-based hybrid photocatalysts with boosted performance toward targeting artificial photoredox applications.

2. Experimental section

2.1. Materials

Chemicals were obtained from Sinopharm Chemical Reagent Co., Ltd. (Shanghai, China), including cadmium chloride ($\text{CdCl}_2 \cdot 2.5\text{H}_2\text{O}$), sodium diethyldithiocarbamate trihydrate ($\text{C}_5\text{H}_{10}\text{NNaS}_2 \cdot 3\text{H}_2\text{O}$), ethylenediamine ($\text{C}_2\text{H}_8\text{N}_2$), thioacetamide ($\text{C}_2\text{H}_5\text{NS}$), sodium molybdate ($\text{Na}_2\text{MoO}_4 \cdot 2\text{H}_2\text{O}$), potassium ferricyanide ($\text{K}_3[\text{Fe}(\text{CN})_6]$), potassium ferrocyanide ($\text{K}_4[\text{Fe}(\text{CN})_6]$), potassium chloride (KCl) and N, N-dimethylformamide (DMF). All materials were analytical grade and used as received without further purification. Deionized water was used throughout this study.

2.2. Materials synthesis

2.2.1. Fabrication of CdS NWs

Uniform CdS NWs were fabricated as in our previous researches [48,49]. The details were presented in the Supporting information (SI).

2.2.2. Construction of 1D CM core-shell nanowires

The 1D CM core-shell nanowires were prepared via a facile hydrothermal method [50,51]. Typically, a certain amount of thioacetamide ($\text{C}_2\text{H}_5\text{NS}$) and sodium molybdate ($\text{Na}_2\text{MoO}_4 \cdot 2\text{H}_2\text{O}$) were dissolved in 40 mL of DI water to form a transparent solution. Then, 50 mg of as-prepared CdS NWs were dispersed in the obtained solution by sonication for 5 min. After stirring for another 60 min, the suspension was transferred to a 50 mL Teflon-lined stainless steel autoclave and then heated in an electric oven at 473 K for 24 h. Subsequently, the products were separated by centrifugation and washed with deionized water and ethanol for three times, respectively, followed by drying at room temperature with a gentle stream of N_2 . The theoretical weight percent of MoS_2 in the 1D CM core-shell nanowires were controlled to be 1, 2, 5 and 10 wt% by changing the amount of $\text{C}_2\text{H}_5\text{NS}$ and $\text{Na}_2\text{MoO}_4 \cdot 2\text{H}_2\text{O}$, and were referred to as C1M, C2M, C5M, and C10M, respectively. For comparison, the various amounts of Pt as cocatalyst were loaded onto the surface of CdS NWs via an in situ photodeposition method using H_2PtCl_6 aqueous solutions as precursor. Analogously, the resultant CdS-Pt composites with various amounts of Pt were denoted as C0.5P, C1P, C2P, respectively. The pure MoS_2 powders were synthesized under the same conditions without the addition of CdS NWs.

2.3. Characterization

The powder X-ray diffraction (XRD) patterns of the samples were recorded on a Bruker D8 Advance powder X-ray diffractometer (40 kV, 40 mA) using Ni-filtered $\text{Cu K}\alpha$ radiation in the 2θ ranging from 10 to 80° at a scan rate of $0.02^\circ \text{ s}^{-1}$. The optical properties of the samples were analyzed by UV-vis diffuse reflectance spectroscopy (DRS) using a UV-vis spectrophotometer (Cary 500, Varian Co.) in which BaSO_4 was employed as the internal

reflectance standard. Field-emission scanning electron microscopy (FE-SEM) was used to determine the morphology of the samples on an FEI Nova NANOSEM 230 spectrophotometer. The transmission electron microscopy (TEM) images and high-resolution transmission electron microscopy (HRTEM) images were obtained using a JEOL model JEM 2010 EX instrument at an acceleration voltage of 200 kV. X-ray photoelectron spectroscopy (XPS) measurements were performed using a Thermo Scientific ESCA Lab250 spectrometer, and all of the binding energies were calibrated by the C 1s peak at 284.6 eV. Nitrogen (N_2) adsorption-desorption isotherms and the Brunauer-Emmett-Teller (BET) surface areas were determined at 77 K using Micromeritics ASAP2010 equipment. The photoluminescence (PL) spectra for solid samples were investigated on an Edinburgh FL/FS900 spectrophotometer with an excitation wavelength of 380 nm.

The photocurrent measurement was carried out on a BAS Epsilon workstation without bias and the electrolyte was 0.2 M aqueous Na_2SO_4 solution ($\text{pH} = 6.8$) without an additive. The visible light irradiation source was a 300 W Xe arc lamp system equipped with a UV-CUT filter ($\lambda > 420 \text{ nm}$). The electrochemical impedance spectroscopy (EIS) measurements were performed in the presence of 5.0 mM $\text{K}_3[\text{Fe}(\text{CN})_6]/\text{K}_4[\text{Fe}(\text{CN})_6]$ by applying an ac voltage with 5 mV amplitude in a frequency range from 1 Hz to 85 kHz under open circuit potential conditions. The cathodic polarization curves were obtained using the linear sweep voltammetry (LSV) technique with a scan rate of 0.2 mV s^{-1} . The details of the preparation of electrodes are presented in the SI.

2.4. Photocatalytic H_2 production

The photocatalytic experiments were carried out in a Pyrex vessel, which was attached a closed gas-circulation and evacuation system. Photoreduction of H_2O to H_2 was performed by dispersing 20 mg of photocatalyst in an 80 mL aqueous solution containing 8 mL lactic acid as the sacrificial agent. The photocatalytic system was thoroughly degassed and irradiated by a 300 W Xe lamp with a UV-CUT filter to cut off light with a wavelength $\lambda < 420 \text{ nm}$. A continuous magnetic stirrer was applied at the bottom of the reactor in order to keep the photocatalyst in suspension status during the whole experiment. The temperature of the reaction solution was maintained at 278 K by a flow of cooling water during the reaction. The evolved H_2 was in situ monitored periodically by an online gas chromatograph with a thermal conductivity detector (Shimadzu GC-8A, argon as a carrier gas and MS-5A column). The experimental set up is shown in Fig. S1.

The recycling test of catalytic H_2 evolution over the photocatalyst was done as follows. Typically, after the reaction of the first run under visible light irradiation, the photocatalytic system was thoroughly degassed again, without the separation of photocatalysts or the supplement of lactic acid. Subsequently, the thoroughly degassed system was irradiated again by a 300 W Xe lamp with a UV-CUT filter to cut off light with a wavelength $\lambda < 420 \text{ nm}$. Analogously, the following three runs of photocatalytic recycling tests were performed.

The apparent quantum yield (A.Q.Y.) was measured under the same photocatalytic reaction condition and irradiated by a 300 W Xe lamp with a 420 nm band-pass filter (MIF-W, Optical Coatings Japan Co., Japan). The number of incident photons was measured using a radiant power energy meter (Ushio spectroradiometer, USR-40). The A.Q.Y. was calculated according to the equation below:

$$\begin{aligned} \text{A.Q.Y.} &= \frac{\text{number of reacted electrons}}{\text{number of incident photons}} \times 100\% \\ &= \frac{\text{number of evolved hydrogen molecules} \times 2}{\text{number of incident photons}} \times 100\% \end{aligned}$$

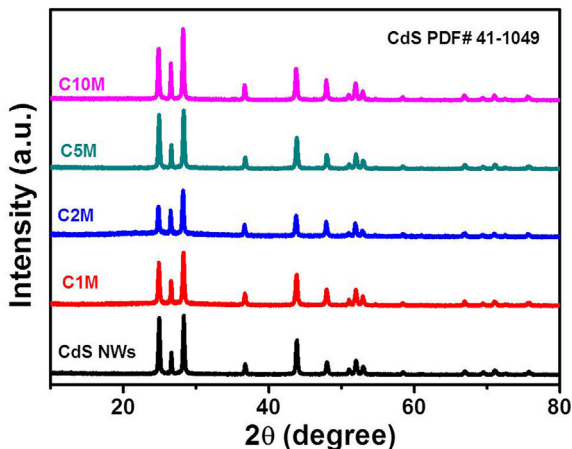


Fig. 1. X-ray diffraction patterns for pure CdS NWs and 1D CdS@MoS₂ (CM) core-shell nanowires loading with various amounts of MoS₂.

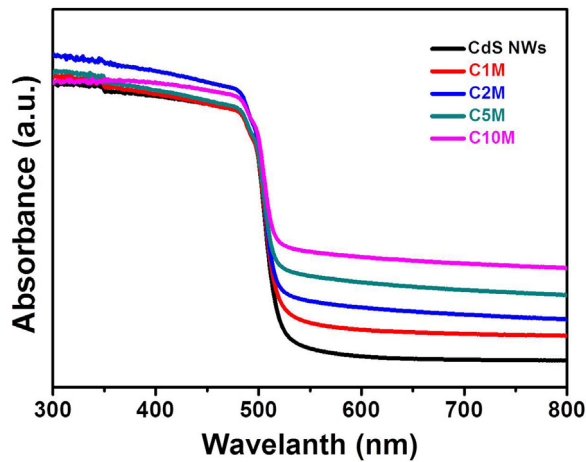


Fig. 2. UV-vis diffuse reflectance spectra (DRS) of pure CdS NWs and 1D CdS@MoS₂ (CM) core-shell nanowires loading with various amounts of MoS₂.

3. Results and discussion

3.1. Formation and characterization

The crystallographic structures of the as-prepared pure CdS NWs and a series of 1D CM heterostructures with various loading amounts of MoS₂ have been collected by using powder X-ray diffraction (XRD), as shown in Fig. 1. It is observed that all samples possess similar XRD patterns, exhibiting diffraction peaks of hexagonal CdS with lattice constants of $a=0.414$ nm and $c=0.672$ nm (PDF#41-1049). Therefore, the results suggest that such a hydrothermal process has no effects on the crystalline structure of CdS NWs. However, no diffraction features related to MoS₂ can be observed, which may be attributed to the low crystallinity, low content and high dispersion of MoS₂ in the composites, as shown in the TEM images below.

Fig. 2 shows UV-vis diffuse reflectance spectra (DRS) of the as-prepared samples. For the pure CdS NWs, a significant absorption at wavelength shorter than 520 nm can be assigned to the intrinsic bandgap absorption [52,53]. It is obvious that loading the MoS₂ cocatalysts onto the surface of 1D CdS nanowires can increase the absorption of catalysts in visible light region from 520 to 800 nm and the absorption of CM composites is enhanced with the increase of MoS₂ content. This is in accordance with the color change of the

samples (Fig. S2). More importantly, few differences arising from the inherent band structure of the CdS NWs can be observed after the hydrothermal process, indicating MoS₂ is deposited onto the surface of CdS nanowires rather than entering crystal grating of CdS NWs. This observation is well consistent with the results of XRD.

The surface morphology of the samples has been checked by field-emission scanning electron microscopy (FE-SEM). Fig. S3A shows that the blank CdS NWs exhibit the highly uniform 1D morphology with an average diameter of ca. 50–100 nm. As depicted in Fig. S3B, the CM sample still keeps the 1D geometry, but the surfaces become rough along the entire length with a myriad of thin nanosheets tightly bounded onto the surface of the nanowires. Notably, blank MoS₂ sample displays the irregular morphology, as shown in Fig. S3C–D. Such a striking difference between the blank MoS₂ and MoS₂ in CM sample suggests that the presence of 1D CdS NWs provides abundant highly accessible interfaces for the growth of MoS₂ thin shell, thereby forming the 1D CdS NWs@MoS₂ (CM) core-shell structure.

In order to further visualize the morphology and microstructure of the as-prepared CM heterostructures, transmission electron microscopy (TEM) has been employed to investigate blank CdS NWs and the C5M sample as an example. Fig. 3A shows that the blank CdS NWs exhibit the highly uniform 1D morphology with an average diameter of ca. 50–100 nm. After the hydrothermal process, as revealed in Fig. 3B, the nanowires still keep their 1D geometry. In Fig. 3B, it is also clearly seen that the 1D CdS is covered by a ca. 5 nm thin shell with a distinct interface between the CdS core and thin shell. The large and intimate interfacial contact between the core and thin shell in such core-shell structures favors the formation of junctions between the two components [54,55], and as a result, drastically facilitates the transfer and separation of photogenerated charge carriers, thereby improving the photocatalytic activity. Fig. 3C shows the high-resolution TEM image (HRTEM) of C5M sample, which displays two fringes with lattice spacings of 0.34 nm and 0.27 nm, corresponding to the (002) facet of hexagonal CdS NWs and the (100) plane of MoS₂, respectively [56,57]. Compared with the well-crystallized CdS NWs, the lattice spacing corresponding to MoS₂ layer is relatively inconspicuous, suggesting the low crystallinity of MoS₂ in the composites. As reflected in Fig. S4, the energy-dispersive X-ray spectrum of a selected area of C5M sample shows the presence of Cd, Mo, and S elements.

The X-ray photoelectron spectrum (XPS) analysis has been carried out to gain insight into the chemical composition and binding states on the surface of the C5M samples. Fig. S5A displays the XPS survey spectrum of the C5M composite, which demonstrates the existence of Cd, S and Mo elements. The typical high-resolution XPS spectrum of Cd 3d delivers two strong peaks at binding energies of 405.4 and 412.2 eV, as shown in Fig. S5B, which are assigned to Cd²⁺ in CdS [58]. As shown in Fig. 4A–B, the doublet peaks at 232.2 and 228.4 eV are ascribed to the binding energy of Mo 3d_{3/2} and 3d_{5/2} orbits for the +4 oxidation state [40,59], while the characteristic peaks of S 2s, S 2p_{1/2} and S 2p_{3/2} orbits are observed at 226.4, 162.4 and 161.1 eV [60,61], respectively, suggesting the existence of S²⁻. Also of note is that the peaks and tailing spectra for Mo⁶⁺ (at about 236 eV) [50] cannot be observed. Therefore, the joint results of DRS, TEM and XPS lead to a conclusion that the well-defined 1D CdS NWs@MoS₂ (CM) core-shell nanowire composites have been successfully prepared via the facile hydrothermal method.

3.2. Visible light-driven H₂ generation

The photocatalytic H₂ production rates of the samples are measured under visible light irradiation with lactic acid as sacrificial reagents, and the results are shown in Fig. 5A. Due to the fast recombination of photogenerated charges and the shortage of activity

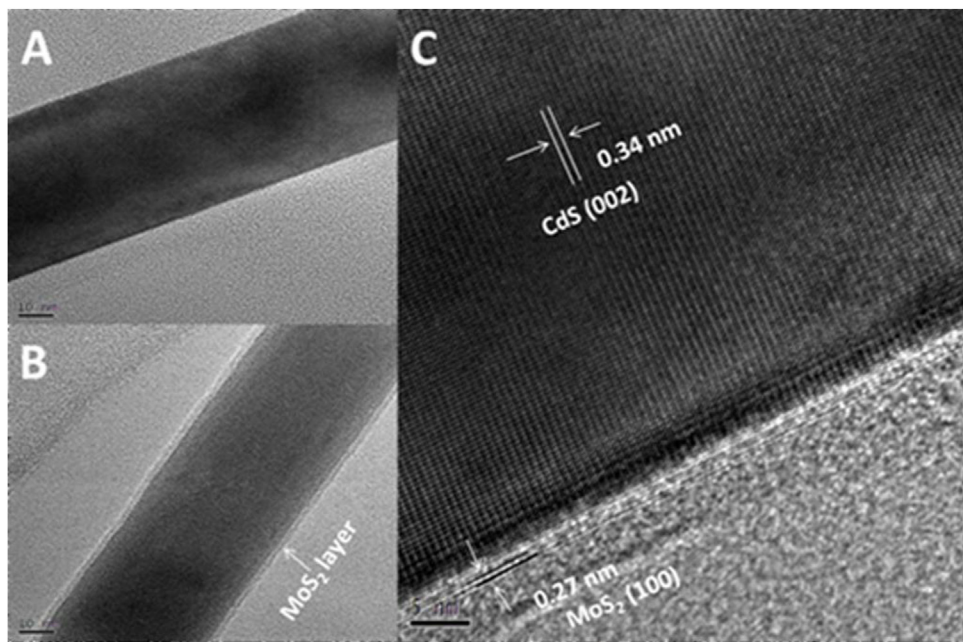


Fig. 3. Typical TEM images of as-prepared samples: blank CdS NWs (A), 1D CdS@5 wt% MoS₂ (C5M) core-shell nanowires (B), and HRTEM image of 1D CdS@5 wt% MoS₂ (C5M) core-shell nanowires (C).

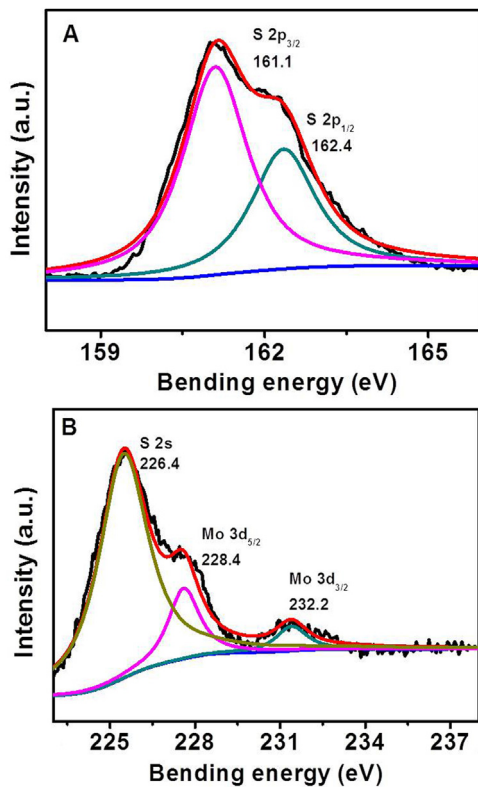


Fig. 4. High-resolution XPS of S 2p (A) and Mo 3d (B) of 1D CdS@5 wt% MoS₂ (C5M) core-shell nanowires.

sites in CdS NWs, bare CdS NWs sample shows a relatively low photocatalytic activity with a H₂ evolution rate of 7.6 $\mu\text{mol h}^{-1}$ during the reaction process. Blank MoS₂ specimen is inactive in this reaction system, which is consistent with previous reports [62,63]. Notably, loading MoS₂ shell onto the surface of CdS NWs is capable of remarkably enhancing the average rates of H₂ evolution. When loading content of MoS₂ is 2 wt%, the H₂ production rate reaches an

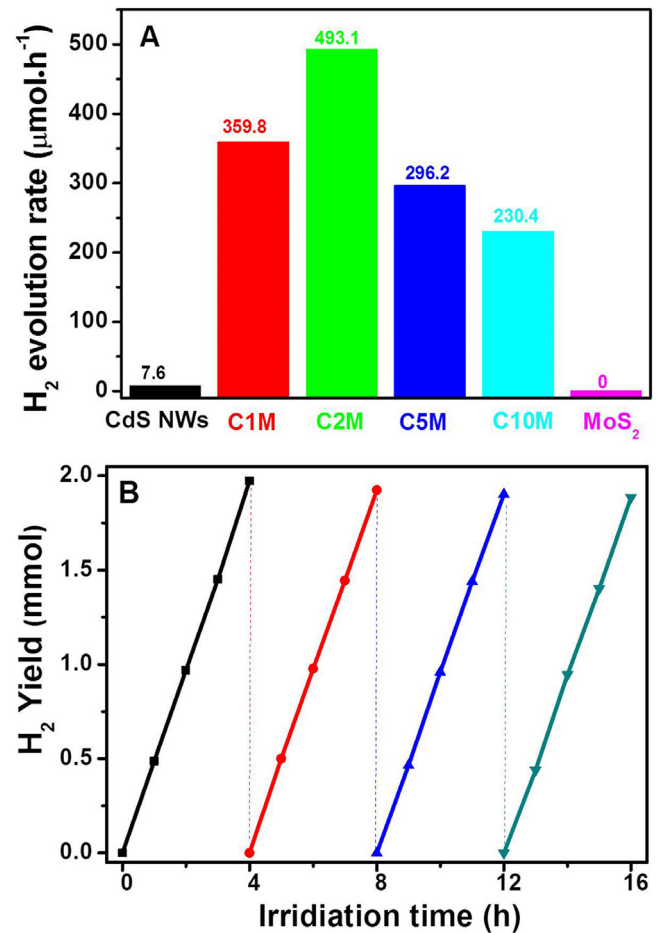


Fig. 5. Comparison of the photocatalytic H₂ production activity of different samples for 4 h (A), the photocatalytic H₂ production stability of 1D CdS@2 wt% MoS₂ (C2M) core-shell nanowires (B).

optimal value of up to $493.1 \mu\text{mol h}^{-1}$, corresponding to an A.Q.Y. of ca. 28.5% at 420 nm. Such an excellent activity is approximately 64 times higher than that of CdS NWs alone (A.Q.Y. = 0.4%). Interestingly, the reaction system produces a large amount of gas bubbles in a cuvette over the C2M photocatalyst, which is easily observable by the naked eye (Movie S1, SI). However, further increasing the content of MoS₂ in hybrids leads to a gradual decrease of H₂ evolution activity, which may originate from the masking effect of MoS₂; that is, the increased light absorption of MoS₂ caused by the higher content would impair the excitation of CdS [64,65]. Therefore, C2M sample is chosen as the example to be investigated in the follow-on works. Also of note is that blank CdS NWs display a relatively low H₂ generation rate in the first hour, as demonstrated in Fig. S6A, indicating the existence of an induced period [3,52,66]. However, this phenomenon is not observed in C2M sample (Fig. S6B), which may be due to the introduction of MoS₂ as efficient water reduction cocatalyst. Since Pt is always employed as efficient cocatalyst towards photocatalytic H₂ generation due to its large work functions [67,68], the H₂ evolution performances of CdS-Pt (CP) composites have also been investigated for comparison under identical conditions. As revealed in Fig. S7, the optimal H₂ evolution rate of CP composites is ca. $86.8 \mu\text{mol h}^{-1}$ with an A.Q.Y. of 4.7%, which is still much lower than that of C2M, indicating that the as-prepared 1D CM core-shell nanowires are excellent systems for photocatalytic H₂ evolution.

Subsequent experiments have been performed to investigate the photocatalytic durability, which is as important as activity from the perspective of application. As depicted in Fig. 5B, the time course of photocatalytic H₂ evolution of the C2M sample has been measured every 4 h as one cycle. It is clear that there is no significant decrease in activity for H₂ production during the tested 4 cycles. Furthermore, the crystal structure of C2M after 16 h of irradiation is analyzed. As revealed in Fig. S8, XRD patterns of the fresh and used samples demonstrate an identical crystalline structure. The complementary characterizations unambiguously indicate that the prepared CM composite is a robust photocatalyst in the present photocatalytic H₂ evolution system.

To explore the influence of reaction conditions on photocatalytic performance, control experiments, including under aerobic conditions and without lactic acid as sacrificial agent, have been further performed with C2M as the example. Interestingly, the C2M photocatalyst without degassing (hereinafter denoted as C2M-O₂) can also exhibit a considerable H₂ evolution rate of $175.8 \mu\text{mol h}^{-1}$ (Fig. S9). Although the activity is lower than that of C2M under vacuum conditions due to the backward reaction of H₂ and O₂ to form H₂O on the photocatalyst surface, it is still higher than that of blank CdS under vacuum conditions. Notably, the degassing effect originated from the constant of H₂ gas [18] and the suppression of reverse reactions due to the loading of MoS₂ [30] may contribute to the activity of C2M-O₂. Fig. S9 demonstrates the photocatalytic activity of C2M in the absence of sacrificial agent, which is denoted as C2M-P. It is clear that C2M-P displays a photocatalytic H₂ evolution rate of $10.1 \mu\text{mol h}^{-1}$, which is still higher than that of pure CdS NWs in lactic acid solution. Such joint results indicate that loading MoS₂ shell onto the surface of 1D CdS NWs is an effective pathway to improve the performance of semiconductors for evolution of H₂ from water splitting.

3.3. Origin of the enhanced performance

To investigate the origin of the enhanced photocatalytic H₂ production over the 1D CM core-shell nanowires photocatalysts, we have then comparatively characterized blank CdS NWs and C2M sample. Fig. 6A shows the polarization curves of blank CdS NWs and C2M sample. The observed cathodic current in the range of

–0.3 to –0.7 V versus Ag/AgCl can be ascribed to the H₂ evolution. Compared with blank CdS NWs, C2M sample displays an enhanced current density. This result indicates that MoS₂ can efficiently promote the photoactivity of reduction of water to H₂. The photoluminescence (PL) spectra have been employed to study the efficiency of the interfacial electron transfer. It is generally recognized that the PL emission results from the recombination of free charge carriers [69,70]. It is clearly observed from Fig. 6B that the CdS NWs sample displays two distinct emission bands at ca. 520 nm and 710 nm, which can be attributed to near-band-edge emission and the excess of sulfur or core defects on the nanowires surfaces, respectively [71,72]. The decreased PL intensity of the C2M composite in compared with pure CdS NWs indicates that the separation efficiency of photo-induced electron-hole pairs is improved by loading MoS₂ thin shell. Notably, the emission band at 710 nm of CdS NWs disappeared after loading MoS₂ shell onto the surface of CdS NWs, indicating the effective passivation effect for the nanowires surface defect states [73–75].

To further evaluate the efficiency of charge carriers transfer and separation, the photocurrent response of both CdS NWs and C2M have been tested. Photocurrent is produced due to the diffusion of photogenerated electrons to the back contact and, meanwhile, the capture of photogenerated holes by electron-donor in the electrolyte [76]. Fig. 6C shows the periodic on/off photocurrent response of the samples under the irradiation of visible light. Apparently, loading MoS₂ thin shell dramatically improves photocurrent density of 1D C2M core-shell nanowires, and the C2M sample exhibits an approximately two-fold enhancement of photocurrent density as compared with blank CdS NWs. The charge transfer and recombination process of photoinduced electrons and holes in the photocatalysts can also be evidenced by the electrochemical impedance spectrum (EIS). As manifested in Fig. 6D, C2M sample shows a distinctly decreased diameter of the semicircular Nyquist plot than blank CdS NWs, indicating a faster charge-carrier transfer rate in the C2M nanocomposites.

The surface area and porosity of the samples, which also play an essential role in the performance of the photocatalysts [77], are investigated. Fig. S10 shows the nitrogen adsorption-desorption isotherm results of CdS NWs and C2M heterostructures. Each isotherm shows the distinct H3 hysteresis loop in a relative pressure range of 0.9–1, which is related to slit-like pores due to the random aggregation of CdS NWs [19,52]. From Fig. S10 and Table S1, it can be observed that loading MoS₂ thin shell onto the surface of CdS NWs can affect the surface area and porosity. The blank CdS NWs display a Brunauer-Emmett-Teller surface area (S_{BET}) of $15.7 \text{ m}^2 \text{ g}^{-1}$. However, the S_{BET} decreases to $8.4 \text{ m}^2 \text{ g}^{-1}$ when loading 2 wt% MoS₂ onto the surface of CdS NWs, and the total pore volume of the samples also reduces from 0.08 to $0.05 \text{ cm}^3 \text{ g}^{-1}$ after loading MoS₂. The surface area and porosity of the samples exhibit a reverse sequence to its photoactivity. Therefore, dramatically enhanced photocatalytic H₂ evolution performance over 1D CM core-shell nanowires should not originate from the variation of surface area and porous structures.

Based on the above results, a tentative reaction mechanism for photocatalytic H₂ evolution from water over the 1D CM core-shell nanowires is proposed and the schematic diagram is illustrated in Scheme 1. Upon visible light irradiation, CdS NWs is excited to produce the electron-hole pairs. The photogenerated charge carriers can quickly recombine within the CdS NWs in the absence of MoS₂ cocatalyst (Scheme 1A), leading to a relatively low activity. When loading MoS₂ shell onto the surface of CdS NWs, there is a strong thermodynamic driving force for electron transfer from the excited CdS NWs core to MoS₂ shell due to the comparable energy difference between their conduction band (CB) (Scheme 1B). More importantly, the large and intimate coaxial interfacial contact between 1D CdS NWs core and MoS₂ thin shell plays an

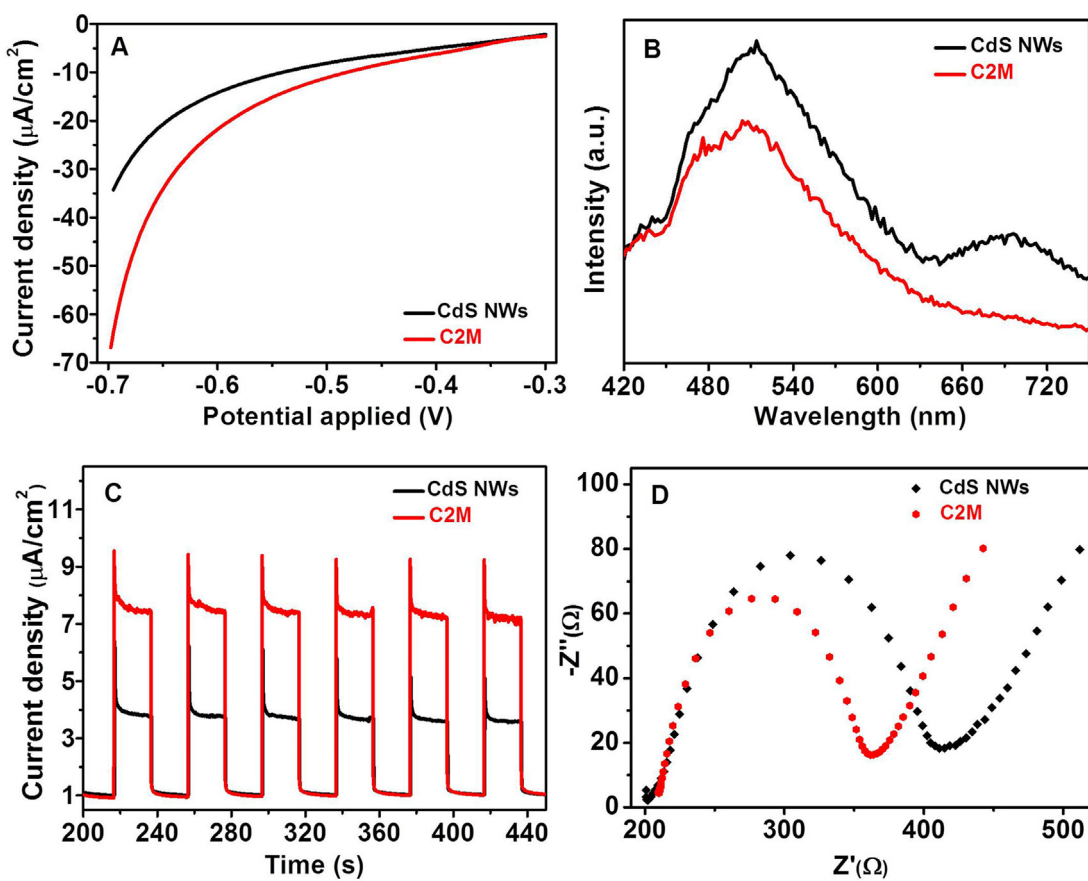
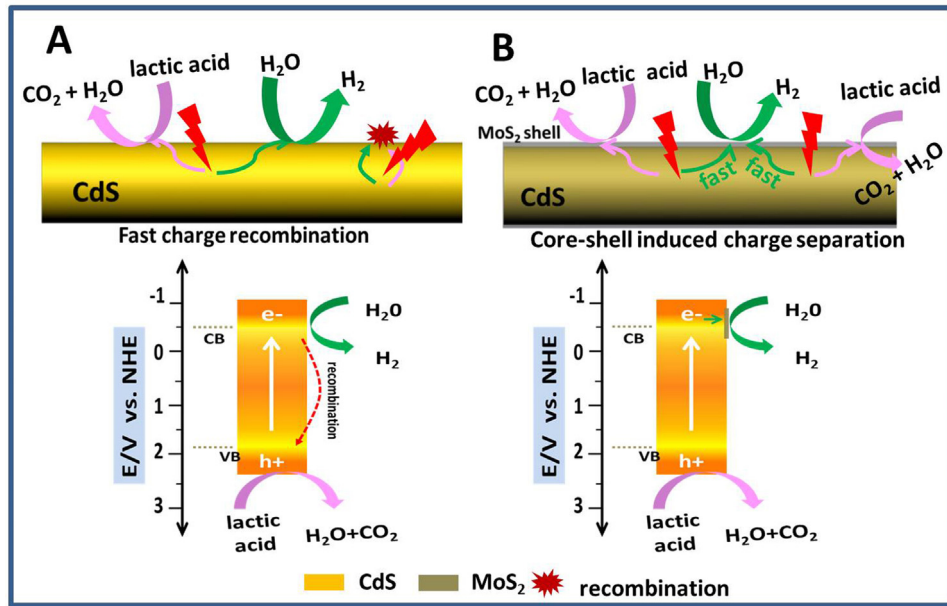


Fig. 6. Polarization curves (A), photoluminescence spectra (B), transient photocurrent responses (C) and electrochemical impedance spectroscopy (EIS) Nyquist plots (D) of bare CdS NWs and 1D CdS@2 wt% MoS₂ (C2M) core-shell nanowires.



Scheme 1. Proposed mechanism for the photocatalytic H₂ generation of the CdS NWs (A) and 1D CM core-shell heterostructures (B) under visible light irradiation with lactic acid as the sacrificial agent.

essential factor in favoring the electrons transfer from CdS core to MoS₂ shell, which also serves as active sites because unsaturated S atoms of MoS₂ have strong bonds to H⁺ in the solution, thereby facilitating the photoactivity enhancement of 1D CM core-shell

nanowires composites toward H₂ evolution. Meanwhile, photogenerated holes in the VB of CdS are trapped by the sacrificial agent, namely lactic acid.

4. Conclusion

In summary, 1D CM core-shell nanowires have been successfully constructed via a facile hydrothermal strategy. The resultant core-shell nanowire composite with optimal loading amount of MoS₂ exhibits the highest H₂ evolution rate of 493.1 $\mu\text{mol h}^{-1}$ with lactic acid as the sacrificial agent, corresponding to an apparent quantum yield (A.Q.Y.) of 28.5% at 420 nm. Such a high activity is ca. 64 and 4 times higher than that of pure CdS NWs and CdS–1 wt% Pt composite, respectively. In the 1D CM core-shell nanowires, MoS₂ thin shell is favorable for markedly transferring photoexcited electrons in CdS NWs core due to the comparable energy difference between their CB, and the intimate coaxial interfacial contact, as well as enriching activity sites for H₂ generation. Hopefully, this work affords a feasible paradigm for the fine design of well-defined 1D-based hybrid photocatalysts towards boosted photocatalytic solar energy conversion.

Acknowledgements

The support by the National Natural Science Foundation of China (NSFC) (20903022, 21173045, and U1463204) and the Science and Technology Development of Foundation of Fuzhou University (2013-XQ-16) is gratefully acknowledged.

Appendix A. Supplementary data

Supplementary data associated with this article can be found, in the online version, at <http://dx.doi.org/10.1016/j.apcatb.2016.09.023>.

References

- [1] N.S. Lewis, D.G. Nocera, Proc. Natl. Acad. Sci. U. S. A. 103 (2006) 15729–15735.
- [2] N. Zhang, M.-Q. Yang, S. Liu, Y. Sun, Y.-J. Xu, Chem. Rev. 115 (2015) 10307–10377.
- [3] Z. Han, F. Qiu, R. Eisenberg, P.L. Holland, T.D. Krauss, Science 338 (2012) 1321–1324.
- [4] L. Li, J. Yan, T. Wang, Z.-J. Zhao, J. Zhang, J. Gong, N. Guan, Nat. Commun. 6 (2015) 5881–5891.
- [5] Y.P. Xie, Z.B. Yu, G. Liu, X.L. Ma, H.-M. Cheng, Energy Environ. Sci. 7 (2014) 1895–1901.
- [6] J.B. Joo, R. Dillon, I. Lee, Y. Yin, C.J. Bardeen, F. Zaera, Proc. Natl. Acad. Sci. U. S. A. 111 (2014) 7942–7947.
- [7] N. Zhang, C. Han, Y.-J. Xu, J.J. Foley IV, D. Zhang, J. Codrington, S.K. Gray, Y. Sun, Nat. Photonics 10 (2016) 473–482.
- [8] Z. Zou, J. Ye, K. Sayama, H. Arakawa, Nature 414 (2001) 625–627.
- [9] L. Yuan, C. Han, M.-Q. Yang, Y.-J. Xu, Int. Rev. Phys. Chem. 35 (2016) 1–36.
- [10] Y. Tachibana, L. Vayssières, J.R. Durrant, Nat. Photonics 6 (2012) 511–518.
- [11] T.-D. Nguyen-Phan, S. Luo, D. Vovchok, J. Llorca, J. Graciani, J.F. Sanz, S. Sallis, W. Xu, J. Bai, L.F.J. Piper, D.E. Polanyky, E. Fujita, S.D. Senanayake, D.J. Stacioli, J.A. Rodriguez, ACS Catal. 6 (2016) 407–417.
- [12] J. Tian, Z. Zhao, A. Kumar, R.I. Boughton, H. Liu, Chem. Soc. Rev. 43 (2014) 6920–6937.
- [13] C. Liu, N.P. Dasgupta, P. Yang, Chem. Mater. 26 (2013) 415–422.
- [14] F.X. Xiao, J. Miao, H.B. Tao, S.F. Hung, H.Y. Wang, H.B. Yang, J. Chen, R. Chen, B. Liu, Small 11 (2015) 2115–2131.
- [15] X. Xu, G. Yang, J. Liang, S. Ding, C. Tang, H. Yang, W. Yan, G. Yang, D. Yu, J. Mater. Chem. A 2 (2014) 116–122.
- [16] G. Yang, W. Yan, Q. Zhang, S. Shen, S. Ding, Nanoscale 5 (2013) 12432–12439.
- [17] Z. Han, G. Chen, C. Li, Y. Yu, Y. Zhou, J. Mater. Chem. A 3 (2015) 1696–1702.
- [18] Z. Sun, H. Zheng, J. Li, P. Du, Energy Environ. Sci. 8 (2015) 2668–2676.
- [19] J. Yu, Y. Yu, P. Zhou, W. Xiao, B. Cheng, Appl. Catal. B: Environ. 156–157 (2014) 184–191.
- [20] J. Yuan, J. Wen, Y. Zhong, X. Li, Y. Fang, S. Zhang, W. Liu, J. Mater. Chem. A 3 (2015) 18244–18255.
- [21] X. Wang, H. Yu, L. Yang, L. Shao, L. Xu, Catal. Commun. 67 (2015) 45–48.
- [22] D. Bao, P. Gao, X. Zhu, S. Sun, Y. Wang, X. Li, Y. Chen, H. Zhou, Y. Wang, P. Yang, Chem. Eur. J. 21 (2015) 12728–12734.
- [23] G. Zhou, X. Xu, T. Ding, B. Feng, Z. Bao, J. Hu, ACS Appl. Mater. Interfaces 7 (2015) 26819–26827.
- [24] K. Maeda, K. Teramura, D. Lu, N. Saito, Y. Inoue, K. Domen, Angew. Chem. 118 (2006) 7970–7973.
- [25] J. Yu, Y. Hai, B. Cheng, J. Phys. Chem. C 115 (2011) 4953–4958.
- [26] J. Yang, H. Yan, X. Wang, F. Wen, Z. Wang, D. Fan, J. Shi, C. Li, J. Catal. 290 (2012) 151–157.
- [27] B.J. Ma, J.S. Kim, C.H. Choi, S.I. Woo, Int. J. Hydrogen Energy 38 (2013) 3582–3587.
- [28] K. Wu, Z. Chen, H. Lv, H. Zhu, C.L. Hill, T. Lian, J. Am. Chem. Soc. 136 (2014) 7708–7716.
- [29] X. Li, W. Bi, L. Zhang, S. Tao, W. Chu, Q. Zhang, Y. Luo, C. Wu, Y. Xie, Adv. Mater. 28 (2016) 2427–2431.
- [30] J. Yang, D. Wang, H. Han, C. Li, Acc. Chem. Res. 46 (2013) 1900–1909.
- [31] L. Liu, Z. Ji, W. Zou, X. Gu, Y. Deng, F. Gao, C. Tang, L. Dong, ACS Catal. 3 (2013) 2052–2061.
- [32] F.E. Osterloh, Chem. Mater. 20 (2007) 35–54.
- [33] A. Indra, P.W. Menezes, K. Kailasam, D. Hollmann, M. Schroder, A. Thomas, A. Bruckner, M. Driess, Chem. Commun. 52 (2016) 104–107.
- [34] T.F. Jaramillo, K.P. Jørgensen, J. Bonde, J.H. Nielsen, S. Horch, I. Chorkendorff, Science 317 (2007) 100–102.
- [35] X. Zong, H. Yan, G. Wu, G. Ma, F. Wen, L. Wang, C. Li, J. Am. Chem. Soc. 130 (2008) 7176–7177.
- [36] S. Min, G. Lu, J. Phys. Chem. C 116 (2012) 25415–25424.
- [37] Q. Xiang, J. Yu, M. Jaroniec, J. Am. Chem. Soc. 134 (2012) 6575–6578.
- [38] M. Nguyen, P.D. Tran, S.S. Pramana, R.L. Lee, S.K. Batabyal, N. Mathews, L.H. Wong, M. Graetzel, Nanoscale 5 (2013) 1479–1482.
- [39] M. Liu, F. Li, Z. Sun, L. Ma, L. Xu, Y. Wang, Chem. Commun. 50 (2014) 11004–11007.
- [40] C. Liu, L. Wang, Y. Tang, S. Luo, Y. Liu, S. Zhang, Y. Zeng, Y. Xu, Appl. Catal. B: Environ. 164 (2015) 1–9.
- [41] Y. Liu, Y.-X. Yu, W.-D. Zhang, J. Phys. Chem. C 117 (2013) 12949–12957.
- [42] Y.-F. Zhao, Z.-Y. Yang, Y.-X. Zhang, L. Jing, X. Guo, Z. Ke, P. Hu, G. Wang, Y.-M. Yan, K.-N. Sun, J. Phys. Chem. C 118 (2014) 14238–14245.
- [43] W. Gao, M. Wang, C. Ran, L. Li, Chem. Commun. 51 (2015) 1709–1712.
- [44] J. Ran, J. Zhang, J. Yu, M. Jaroniec, S.Z. Qiao, Chem. Soc. Rev. 43 (2014) 7787–7812.
- [45] K. Chang, Z. Mei, T. Wang, Q. Kang, S. Ouyang, J. Ye, ACS Nano 8 (2014) 7078–7087.
- [46] H. Zhao, Y. Dong, P. Jiang, H. Miao, G. Wang, J. Zhang, J. Mater. Chem. A 3 (2015) 7375–7381.
- [47] J. Xiong, Y. Liu, D. Wang, S. Liang, W. Wu, L. Wu, J. Mater. Chem. A 3 (2015) 12631–12635.
- [48] S. Liu, M.-Q. Yang, Y.-J. Xu, J. Mater. Chem. A 2 (2014) 430–440.
- [49] B. Weng, S. Liu, N. Zhang, Z.-R. Tang, Y.-J. Xu, J. Catal. 309 (2014) 146–155.
- [50] W. Zhou, Z. Yin, Y. Du, X. Huang, Z. Zeng, Z. Fan, H. Liu, J. Wang, H. Zhang, Small 9 (2013) 140–147.
- [51] B. Weng, X. Zhang, N. Zhang, Z.-R. Tang, Y.-J. Xu, Langmuir 31 (2015) 4314–4322.
- [52] J. Yuan, J. Wen, Q. Gao, S. Chen, J. Li, X. Li, Y. Fang, Dalton Trans. 44 (2015) 1680–1689.
- [53] S. Liu, Z. Chen, N. Zhang, Z.-R. Tang, Y.-J. Xu, J. Phys. Chem. C 117 (2013) 8251–8261.
- [54] X. Zhan, Q. Wang, F. Wang, Y. Wang, Z. Wang, J. Cao, M. Safdar, J. He, ACS Appl. Mater. Interfaces 6 (2014) 2878–2883.
- [55] L. Tsakalakos, Mater. Sci. Eng. R-Rep. 62 (2008) 175–189.
- [56] B. Han, S. Liu, Y.-J. Xu, Z.-R. Tang, RSC Adv. 5 (2015) 16476–16483.
- [57] Y. Liu, S. Xie, H. Li, X. Wang, ChemCatChem 6 (2014) 2522–2526.
- [58] Z. Yan, X. Yu, A. Han, P. Xu, P. Du, J. Phys. Chem. C 118 (2014) 22896–22903.
- [59] Y. Li, H. Wang, S. Peng, J. Phys. Chem. C 118 (2014) 19842–19848.
- [60] M.-Q. Yang, C. Han, Y.-J. Xu, J. Phys. Chem. C 119 (2015) 27234–27246.
- [61] T. Jia, A. Kolpin, C. Ma, R.C.-T. Chan, W.-M. Kwok, S.C.E. Tsang, Chem. Commun. 50 (2014) 1185–1188.
- [62] Y.-J. Yuan, Z.-J. Ye, H.-W. Lu, B. Hu, Y.-H. Li, D.-Q. Chen, J.-S. Zhong, Z.-T. Yu, Z.-G. Zou, ACS Catal. 6 (2015) 532–541.
- [63] D. Lang, T. Shen, Q. Xiang, ChemCatChem 7 (2015) 943–951.
- [64] Y. Yuan, H. Lu, F. Wang, B. Hu, Z.T. Yu, Z.-G. Zou, Dalton Trans. 44 (2015) 10997–11003.
- [65] L. Shen, M. Luo, Y. Liu, R. Liang, F. Jing, L. Wu, Appl. Catal. B: Environ. 166–167 (2015) 445–453.
- [66] Z.-J. Li, X.-B. Li, J.-J. Wang, S. Yu, C.-B. Li, C.-H. Tung, L.-Z. Wu, Energy Environ. Sci. 6 (2013) 465–469.
- [67] F. Wang, Y. Jiang, D.J. Lawes, G.E. Ball, C. Zhou, Z. Liu, R. Amal, ACS Catal. 5 (2015) 3924–3931.
- [68] L. Qi, J. Yu, M. Jaroniec, Phys. Chem. Chem. Phys. 13 (2011) 8915–8923.
- [69] Z. Sun, Q. Yue, J. Li, J. Xu, H. Zheng, P. Du, J. Mater. Chem. A 3 (2015) 10243–10247.
- [70] J.G. Radich, N.R. Peebles, P.K. Santra, P.V. Kamat, J. Phys. Chem. C 118 (2014) 16463–16471.
- [71] S. Liu, N. Zhang, Z.-R. Tang, Y.-J. Xu, ACS Appl. Mater. Interfaces 4 (2012) 6378–6385.
- [72] Y. Li, H. Liao, Y. Ding, Y. Fan, Y. Zhang, Y. Qian, Inorg. Chem. 38 (1999) 1382–1387.
- [73] S. Liu, M.-Q. Yang, Z.-R. Tang, Y.-J. Xu, Nanoscale 6 (2014) 7193–7198.
- [74] P. Parkinson, H.J. Joyce, Q. Gao, H.H. Tan, X. Zhang, J. Zou, C. Jagadish, L.M. Herz, M.B. Johnston, Nano Lett. 9 (2009) 3349–3353.
- [75] C.K. Yong, K. Noori, Q. Gao, H.J. Joyce, H.H. Tan, C. Jagadish, F. Giustino, M.B. Johnston, L.M. Herz, Nano Lett. 12 (2012) 6293–6301.
- [76] F.-X. Xiao, S.-F. Hung, J. Miao, H.-Y. Wang, H. Yang, B. Liu, Small 11 (2015) 554–567.
- [77] M. Cao, P. Wang, Y. Ao, C. Wang, J. Hou, J. Qian, Dalton Trans. 44 (2015) 16372–16382.